Green Chemistry

PAPER

View Article Online
View Journal | View Issue

Cite this: *Green Chem.*, 2023, **25**, 5489

Electrocatalysis as an efficient alternative to thermal catalysis over PtRu bimetallic catalysts for hydrogenation of benzoic acid derivatives†

Yan Du, Xiao Chen, * Weilin Shen, Huibin Liu, Min Fang, Jinxuan Liu and Changhai Liang *

The electrocatalytic hydrogenation of aromatic rings in benzoic acid derivatives has arisen as a notionally engaging substitute for thermal catalysis under mild conditions. However, the utilization of organic solvents and low faradaic efficiency are incompatible with the principles of green chemistry and energy conservation. Herein, bimetallic PtRu supported on carbon paper developed by co-electrodeposition with optimized atomic ratios maintains an inspiring high conversion of 92.9%, high selectivity of 100% and a high faradaic efficiency of 62.2% for the hydrogenation of benzoic acid to cyclohexanecarboxylic acid in an acidic aqueous electrolyte without external H_2, which is the best result to date. The optimized electrocatalyst also exhibits outstanding stability and universality for the electrocatalytic hydrogenation of benzoic acid derivatives. *In situ* Raman results and theoretical calculations prove that the synergistic effect generated by Ru modifying the electronic structure of Pt simultaneously enhances the capture of benzoic acid molecules and interfacial active hydrogen species and lowers the reaction energy barrier. After adsorbing benzoic acid, more accumulation of electrons around the Ru atom reduces the electron density of phenyl, thereby activating the reaction. Meanwhile, the uniform alloy nanoclusters anchored to the carbon paper surface ensure highly efficient electronic transmission and high dispersion of active components, reducing excessive agglomeration. A proton-exchange membrane reactor is also used to certify the potential of the electrocatalytic hydrogenation of benzoic acid derivatives for large-scale application.

Received 9th May 2023,
Accepted 26th June 2023

DOI: 10.1039/d3gc01540h

rsc.li/greenchem

Introduction

The selective hydrogenation of aromatic rings in benzoic acid derivatives to form downstream products as fine chemicals, intermediates, and industrial raw materials over heterogeneous catalysts has received much attention.[1–3] For example, cyclohexanecarboxylic acid, produced by the selective hydrogenation of benzoic acid, is an essential organic intermediate for pharmaceuticals such as praziquantel, caprolactam, and ansatrienin, as well as a significant step in the industrial production of nylon-6.[3,4] However, the reaction conditions for benzoic acid hydrogenation to cyclohexanecarboxylic acid are more stringent due to the high resonance energy of electron-deficient aromatic rings, leading to side reactions (carboxyhydrogenation and over-hydrogenation), which makes the highly selective conversion of benzoic acid to cyclohexanecarboxylic acid a challenge.[5–7]

In order to develop an efficient process, the technology of thermal catalytic hydrogenation (TCH) of benzoic acid is commonly used toward cyclohexanecarboxylic acid.[2–4] However, TCH is often subjected to unsafe and environmentally unfavorable operating conditions, including high temperature, high pressure, and an extra supply of H_2 as the hydrogen source (Fig. 1). Additionally, organic solvents such as hexane, cyclohexane, and tetrahydrofuran are probably employed in the TCH process.[3,8,9] Xu *et al.* reported palladium nanoparticles supported on N-doped carbon that achieved a conversion for benzoic acid of 50% and a selectivity for cyclohexanecarboxylic acid of 100% within 24 h.[2] Guo *et al.* synthesized Pt/TiO_2 on account of the strong metal–support interaction effect and realized the conversion of benzoic acid to cyclohexanecarboxylic acid at 80 °C and 5 MPa H_2 in hexane.[3] Therefore, alternative approaches for implementing cyclohexanecarboxylic acid production under more moderate and less polluting conditions are worth investigating.

State Key Laboratory of Fine Chemicals & Laboratory of Advanced Materials and Catalytic Engineering, School of Chemical Engineering, Dalian University of Technology, Dalian 116024, China. E-mail: xiaochen@dlut.edu.cn, changhai@dlut.edu.cn

† Electronic supplementary information (ESI) available. See DOI: https://doi.org/10.1039/d3gc01540h

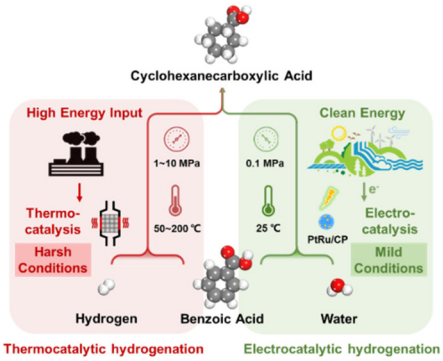

Fig. 1 The characteristics for the electrocatalytic hydrogenation (ECH) process of benzoic acid compared with the traditional thermocatalytic hydrogenation (TCH) process.

In contrast to the TCH process, electrocatalytic hydrogenation (ECH) has drawn extensive research interest,[10–14] which is powered by electricity generated from renewable energy, such as solar and wind power, and achieves the shift from a harsh process to an atmospheric-pressure and room-temperature conversion, thereby meeting the requirements of sustainable energy production.[15–18] Furthermore, aqueous feedstocks are typically adopted as the source of hydrogen, generating oxidative or reducing equivalents without wasteful, potentially toxic reagents.[19–21] Nevertheless, there are still problems and improvements in the hydrogenation conversion of benzoic acid to cyclohexanecarboxylic acid by electrochemical techniques. Fukazawa *et al.* presented the utilization of a proton-exchange membrane reactor over PtRu/Ketjenblack, despite high selectivity and current efficiency towards cyclohexanecarboxylic acid, involving external H_2 and 1,4-dioxane as a solvent.[22] Indeed, the reaction rate of benzoic acid was very low owing to the slow flow rate. Recently, Kong *et al.* considered that commercial platinum carbon electrodes on carbon fiber paper achieved both the benzoic acid conversion and the cyclohexanecarboxylic acid selectivity of 100% without H_2.[23] However, the faradaic efficiency (FE) is approximately 10%, indicating that more electrical energy is dedicated to the accompanying H_2 evolution reaction (HER), which is a common challenge given that it is hard to impede the interaction of protons with charged surfaces without impacting hydrogenation. Evidently, there is a great scope for the enhancement of FE by establishing a more efficient and greener ECH system in the field of converting benzoic acid derivatives.

Herein, a series of PtRu nanocluster electrocatalysts supported on carbon paper (CP) is developed by electrochemical co-deposition for the ECH of benzoic acid. This synthesis method enables the fabrication of uniformly loaded electrode materials with high dispersion of active components anchored to the substrate surface, which reduces excessive agglomeration of active ingredients and improves the electrode stability. Notably, the optimized PtRu/CP simultaneously exhibits high conversion, high selectivity, and high FE to cyclohexanecarboxylic acid, which outperforms previously reported electrocatalysts. The vital role of alloy construction and profound insights into the mechanism for the ECH of benzoic acid are revealed through electrochemical measurements, *in situ* Raman spectroscopy, and density functional theory (DFT). In addition, the ECH of benzoic acid derivatives and the proton-exchange membrane reactor are investigated to verify the high efficiency of PtRu/CP catalysts towards a wide substrate scope and their potential for large-scale production of cyclohexanecarboxylic acid.

Results and discussion

Electrodeposition permits the convenient fabrication of strongly attached electrocatalysts on a conductive base in one step, which effectively evades the coverage of active sites by binders and the loss of active components during the electrochemical reaction. To achieve uniform loading of catalyst nanoparticles, a series of PtRu electrocatalysts with different ratios of metal atoms are prepared *via* a one-step cyclic voltammetry (CV) electrodeposition strategy (Scheme 1) for the ECH of benzoic acid. CP is used as the support material considering that high graphitization degrees of CP enable high dispersion of catalysts and unique electronic interaction, which benefits the adsorption and activation of substrate molecules compared with carbon cloth.[23] PtRu/CP-2, PtRu/CP-4, and PtRu/CP-6 are obtained by adding 2 mM, 4 mM, and 6 mM ruthenium metal salts to the electroplating solution with a fixed concentration of 10 mM platinum metal salt, respectively. Monometallic Pt/CP, Ru/CP, and two-step-deposited Pt/Ru/CP are also synthesized for comparison.

Initially, the ECH of benzoic acid is employed using a separated H-cell with 0.2 M H_2SO_4 solution as the electrolyte, and the cathode compartment includes 10 mM benzoic acid. The as-obtained samples are utilized for working electrodes at a constant current of −50 mA and 120 min (360 charge) at room temperature to determine the catalytic activity (Table 1). The absence of metal active sites on CP contributes to the absolute incapability of benzoic acid conversion. The hydrogenation activity over Pt/CP is significantly higher than that over Ru/CP, with a conversion of 51.7% and 5.8%, respectively. The difference in performance resulting from metallic elements is attributed to the excellence of Pt as catalytically active sites.[24] Pt/Ru/CP exhibits a conversion of 34.1%, slightly improving over Pt/CP. Unexpectedly, the conversion and FE toward cyclohexanecarboxylic acid remarkably increase using PtRu/CP-*X*, where

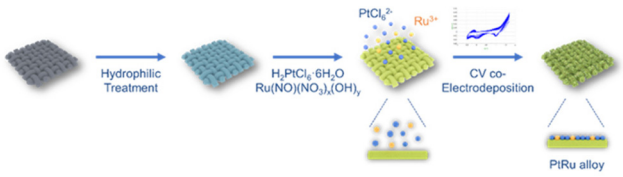

Scheme 1 Schematic illustration of the synthetic strategy for PtRu/CP-*X*.

Table 1 ECH and TCH of benzoic acid over the as-obtained and reported catalysts[a]

Catalyst	Method	Hydrogen source	Pre. (MPa)	Temp. (°C)	Solvent	Current (mA)	Time (min)	Conv. (%)	Sel. (%)	FE (%)	Space–time yield (g m^{-3} h^{-1})
CP	ECH	Water	AP	RT	Water	−50	120	0	0	0	0
Pt/CP	ECH	Water	AP	RT	Water	−50	120	51.7	100.0	20.8	331
Ru/CP	ECH	Water	AP	RT	Water	−50	120	5.8	100.0	3.3	37
Pt/Ru/CP	ECH	Water	AP	RT	Water	−50	120	57.3	100.0	23.1	367
PtRu/CP-2	ECH	Water	AP	RT	Water	−50	120	82.5	100.0	33.2	528
PtRu/CP-4	ECH	Water	AP	RT	Water	−50	120	98.6	100.0	39.6	631
PtRu/CP-6	ECH	Water	AP	RT	Water	−50	120	77.1	100.0	31.0	493
PtRu/CP-4	ECH	Water	AP	RT	Water	−30	120	92.9	100.0	62.2	595
PtRu/Ketjenblack[22]	ECH	H_2	AP	RT	1,4-Dioxane	−6	66.7	1.0	100.0	99.0	576
Pt/CFC[23]	ECH	Water	AP	RT	Water	−40	180	100.0	100.0	10.0	150
Pd@CN[2]	TCH	H_2	AP	85	Water		1440	50.0	100.0		
Pt/TiO_2 [3]	TCH	H_2	5.0	80	Hexane		60	90.0	99.0		
RuPd/CN[25]	TCH	H_2	5.0	100	Water		120	100.0	100.0		
$Rh/NaNbO_3$ [26]	TCH	H_2	0.5	RT	Water		300	100.0	100.0		

[a] Reaction conditions: 0.2 M H_2SO_4 containing 10 mM benzoic acid.

PtRu/CP-4 achieves both the highest conversion and FE at 98.6% and 39.6%, respectively, and the activity follows a volcano-shaped curve with the increased content of Ru in the catalyst. All the as-obtained electrocatalysts show 100% selectivity for cyclohexanecarboxylic acid without hydrogenation of the carboxyl group. Such PtRu catalysts take advantage of this to enhance the activity for the ECH of benzoic acid to cyclohexanecarboxylic acid, probably contributing to the existence of a synergistic effect between bimetallic catalysts. As summarized in Table 1, in contrast to TCH operating at a high temperature and pressure with extra H_2 input, ECH can be realized at room temperature and atmospheric pressure in water, which also entirely consumes benzoic acid in a relatively short time. Notably, the space–time yield over PtRu/CP-4 reported here is much higher than that previously reported by the electrochemical approach. In brief, the ECH strategy delivers a prospective concept for the selective hydrogenation of benzoic acid under mild conditions.

The influence of reaction conditions on activity is further examined systematically over PtRu/CP-4. The conversion of benzoic acid and FE faintly increase within the current range of −20 to −30 mA and show an inconspicuous drop between −30 and −60 mA (Fig. S1†). The selectivity toward cyclohexanecarboxylic acid at various currents remains 100%. Particularly, −30 mA is the optimized current with relatively excellent reaction performance. The electrolytic current is too small, probably resulting in a deficient driving force. While the HER, the competitive response of ECH, becomes dominant at a high current. In this case, adsorbed hydrogen (H_{ad}) on the electrode surface predisposes to the generation of H_2 rather than hydrogenation, consequently diminishing the FE of the reaction. By assigning −30 mA as the electrolysis current, the conversion of benzoic acid is gradually improved and reaches 98.5% within 150 min (Fig. 2a), where the generated product is still all cyclohexanecarboxylic acid. FE shows a minor decrease during the first 120 min and a noticeable decline from 62.2% to 52.8% at 120 min to 150 min, since the concentration of benzoic acid in the electrolyte falls as the reaction time prolongs, resulting in reduced coverage of benzoic acid molecules on the electrode surface and the occurrence of a more severe HER. Evidently, 120 min is the desirable reaction time with a conversion of 92.9% and a FE of 62.2%. The stability experiment of PtRu/CP-4 is explored through five electrolysis cycles at a current of −30 mA for 120 min. As shown in Fig. 2b, the conversion of benzoic acid and FE remain ~90% and ~60%, respectively, suggesting the outstanding stability of the as-prepared PtRu/CP-4. As shown in Fig. S2,† the volumes of H_2 created by the inevitable side reaction are also measured *via* a drainage method for accuracy. About 11 mL H_2 is collected at the end of

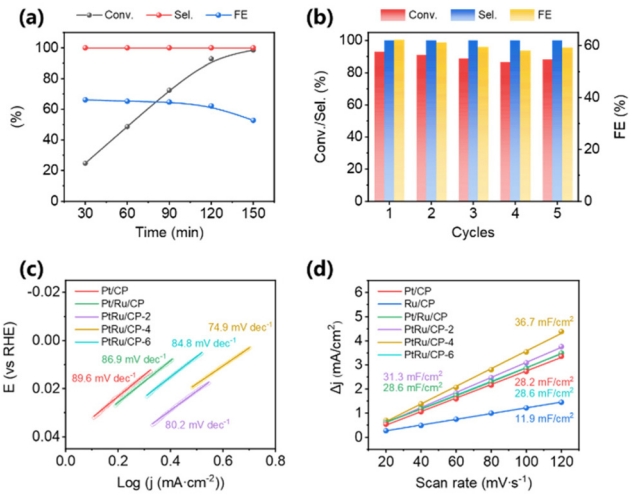

Fig. 2 (a) Conversion (Conv.) of benzoic acid, selectivity (Sel.), and faradaic efficiency (FE) of cyclohexanecarboxylic acid with reaction time at optimized −30 mA. Conditions: 0.2 M H_2SO_4, 10 mM benzoic acid. (b) Five electrolysis cycles over PtRu/CP-4. Conditions: 0.2 M H_2SO_4, 10 mM benzoic acid, −30 mA, 120 min. (c) Tafel slopes in 0.2 M H_2SO_4 with 10 mM benzoic acid. (d) C_{dl} for the as-obtained electrocatalysts in 0.2 M H_2SO_4.

each cycle, and no products other than cyclohexanecarboxylic acid, such as benzaldehyde and benzyl alcohol, are detected by gas chromatography. The total sum of FE for cyclohexanecarboxylic acid and H_2 is close to 100%. Furthermore, large current electrolysis is conducted at −100 mA and −200 mA using PtRu/CP-4, in both cases with an accelerated reaction speed (Fig. S3†). It shows a conversion of 91.1% and a FE of 36.6% at −100 mA within 60 min. When switching the current to −200 mA, benzoic acid gets converted in a shorter time with 93.7% conversion and 28.3% FE within 40 min. Overall, PtRu/CP-4 materializes the best performance for the ECH of benzoic acid to date (Table 1) and the highest space–time yield of 595 g m^{-3} h^{-1}.

Electrochemical tests using the as-obtained catalysts in an undivided three-electrode cell are performed and compared. Linear sweep voltammetry (LSV) tests are conducted in 0.2 M H_2SO_4 with and without 10 mM benzoic acid. As summarized after *iR* compensation in Fig. S4 and Table S1,† the polarization curve of Ru/CP shows a lower catalytic current in 0.2 M H_2SO_4, whereas Pt/CP possesses much higher activity for the HER with almost no difference from Pt/Ru/CP. Notably, three PtRu/CP-*X* samples display slight improvement at −10 mA cm^{-2} current density, where PtRu/CP-4 is the most active. Except for Ru/CP, the LSV curves over all the samples shift to the positive direction in the presence of benzoic acid, suggesting that the ECH of benzoic acid is more inclined to occur than the HER. The voltage change ($\Delta\eta_{10}$) with or without benzoic acid at −10 mA cm^{-2} is used to assess ECH properties.[24] The $\Delta\eta_{10}$ of PtRu/CP-*X* is higher than that of Pt/CP and Pt/Ru/CP, that is, the offset degree of these three samples is more distinctive than that of those two, indicating bimetallic PtRu with superior hydrogenation ability. By means of LSV profiles, the corresponding Tafel plots are acquired to investigate the kinetics for the ECH of benzoic acid over the as-obtained electrocatalysts (Fig. 2c). The slopes express the order Pt/CP > Pt/Ru/CP > PtRu/CP-6 > PtRu/CP-2 > PtRu/CP-4, which declines with the addition of Ru, suggesting that the synergistic effect of bimetallic electrocatalysts dramatically boosts the reaction kinetics. The fastest benzoic acid reduction kinetics on the PtRu/CP-4 surface implies the best capacity to employ H_{ad} produced by the Volmer step of the HER (H_{ad} produced by proton reduction). To evaluate the relative electrochemically active surface area (ECSA), double-layer capacitance (C_{dl}) based on CV measurements is conducted for elucidation of differences in electrocatalyst activity (Fig. S5†). As shown in Fig. 2d, the C_{dl} of PtRu/CP-4 is 36.7 mF cm^{-2}, which is the greatest among bimetallic PtRu electrocatalysts, almost 1.3 times and 3.1 times higher than that of Pt/CP (28.2 mF cm^{-2}) and Ru/CP (11.9 mF cm^{-2}), respectively, implying that PtRu/CP-4 is conferred with an expanded ECSA and greater exposure of active sites on the surface. These possibly contribute to the mass transfer on the electrode surface, thus enhancing the reaction activity. Electrochemical impedance spectroscopy (EIS) measurements are also performed to estimate the efficiency of charge transmission, and Fig. S6† presents the corresponding Nyquist plots of six electrocatalysts. The charge transfer resistance (R_{ct}) obtained from the fitted semicircles shows that PtRu/CP-4 has the lowest R_{ct} among all the samples, indicating a faster electron transfer at the interface of PtRu/CP-4 and the electrolyte.

To certify the universal application of PtRu/CP-4, the ECH of benzoic acid derivatives is conducted under mild conditions (Table 2); the original gas chromatography-mass spectrometry (GC-MS) spectra of products for substrate scopes are shown in Fig. S7–S17.† All the tested substrates undergo aromatic-ring hydrogenation without hydrogenation of the carboxyl group. *o*-Methyl benzoic acid is investigated at −50 mA at room temperature, and 92.0% conversion is acquired in 9 h with a *cis*-isomer of 90.9% selectivity. Clearly, the structure of *o*-methyl benzoic acid is more complicated than that of benzoic acid, demanding a longer time to consume. A high reaction temperature is advantageous to improve the dissolution and mass transfer of the substrate in the electrolyte. Therefore, the time for reaching the equivalent conversion is reduced to 6 h at 50 °C. The hydrogenation of the aromatic rings of *m*-methyl benzoic acid and *p*-methyl benzoic acid can also be achieved, and the selectivity of the *cis*-product is greater than 90%. For *o*-ethyl benzoic acid, the *cis*/*trans* ratio for the products of aromatic ring hydrogenation improves to 99.6/1.4 with practically full conversion. In general, the hydrogenation of the above substrates accomplishes a high stereoselectivity of *cis*-isomers, probably explained by the steric hindrance effect.[4] The ECH reaction is widely perceived to follow the Langmuir–Hinshelwood (L–H) mechanism.[27] The H_{ad} on the metal electrode surface can be believed to attack the substrate molecule adsorbed on the electrocatalyst from the ipsilateral direction, and the *cis*-isomer is the major product. *o*-Trifluoromethylbenzoic acid, which possesses a more electron-deficient aromatic ring, is also implemented for hydrogenation with a *cis*/*trans* ratio of 87.9/12.1. Nevertheless, the presence of trifluoromethyl is drastically negative for the reaction rate, and only 33.5% conversion is realized in 6 h, resembling the published results.[3,22] However, 99.7% conversion with the same selectivity can be achieved by extending the reaction time to 20 h. It should be noted that even dicarboxylic acid with a relatively massive functional group, *e.g.*, phthalic acid, can also be hydrogenated to the corresponding products of aromatic ring saturation under far milder conditions than TCH. Phthalide undergoes electrochemical hydrogenation as well, showing a more efficient process than that of phthalic acid. The selectivity of *cis*-hexahydrophthalide is reduced to 75.7% owing to the formation of by-products with the cleavage of C–O bonds. In addition, the reaction is also suitable for benzoic acid with common functional groups, such as 1-naphthoic acid, methyl benzoate, and anisole, but the reaction conditions should be finely optimized. These results provide an essential implication for the ECH of aromatic model compounds containing polyfunctional groups and imply the highly efficient hydrogenation capability of PtRu/CP-4.

To investigate the structure of electrocatalysts, X-ray diffraction (XRD) patterns of the as-obtained electrodes are presented

Table 2 Electrocatalytic hydrogenation of benzoic acid derivatives over PtRu/CP-4

Entry	Substrate	Product	Current (mA)	Temp. (°C)	Time (h)	Conv. (%)	FE (%)	Sel. (%)
1[a]			−50	RT	9	92.0	8.2	*cis* 90.9 *trans* 9.2
			−50	50	6	92.3	12.4	*cis* 92.2 *trans* 7.8
2[a]			−50	50	6	96.9	12.9	*cis* 96.2 *trans* 3.8
3[b]	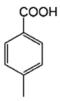	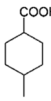	−50	50	3	99.2	5.3	*cis* 96.5 *trans* 3.5
4[a]			−50	50	6	91.6	12.3	*cis* 98.6 *trans* 1.4
5[a]			−50	50	6	33.5	4.3	*cis* 87.9 *trans* 12.1
6[a]			−50	50	20	99.7	4.0	*cis* 87.9 *trans* 12.1
7[a]	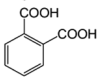		−100	50	9	92.2	4.1	*cis* 96.3 *trans* 3.7
8[c]			−100	50	4	100.0	10.4	*cis* 75.7 *trans* 4.6 (Others[d] 19.7)
9[e]			−50	50	2	100.0	2.5	91.9
10[e]			−50	50	4	100.0	3.1	91.5
11[a]	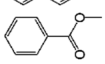	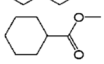	−50	RT	4	96.8	17.9	92.0 (Others[d] 8.0)
12[a]			−50	RT	2	91.2	30.2	82.5 (Others[d] 17.5)

[a] Reaction conditions: H-cell, 1 mL ethanol, 24 mL of 0.2 M H_2SO_4, 10 mM substrate. [b] Reaction conditions: H-cell, 1 mL ethanol, 24 mL of 0.2 M H_2SO_4, 2 mM substrate. [c] Reaction conditions: H-cell, 1 mL ethanol, 24 mL of 0.2 M NaCl, 10 mM substrate. [d] Others refer to the products by the cleavage of C–O bonds. [e] Reaction conditions: H-cell, 5 mL ethanol, 20 mL of 0.2 M H_2SO_4, 1 mM substrate.

in Fig. 3a. With respect to all samples containing platinum, the diffraction peaks at around 40°, 46°, and 68° correspond to the lattice planes (111), (200), and (220) of the face-centered cubic (fcc) structured platinum (JCPDS no. 04-0802), respectively. Apart from the characteristic peak of CP, there is no other impurity phase in the pattern. Concerning PtRu/CP-*X* (*X* = 2, 4, 6), the broadening of XRD peaks and a slight shift of the Bragg angles to higher values compared to pure Pt demonstrate the formation of bimetallic alloys through the incorporation of Ru atoms into the Pt crystal lattice.[28,29] Specifically,

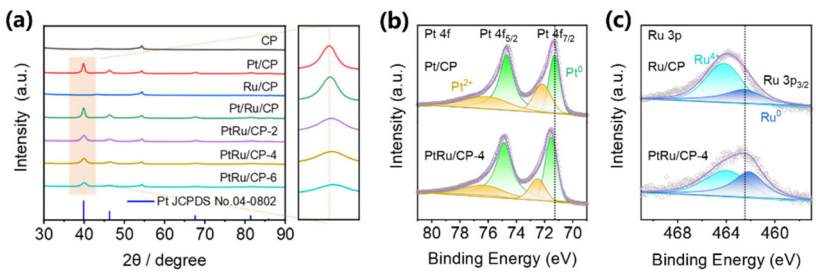

Fig. 3 (a) XRD patterns of CP, Pt/CP, Ru/CP, Pt/Ru/CP, PtRu/CP-2, PtRu/CP-4, and PtRu/CP-6. (The right illustration is a partially magnified image of the tagged section.) (b) Pt 4f, and (c) Ru 3p XPS spectra of Pt/CP, Ru/CP, and PtRu/CP-4.

the position of the (110) peak rises with increasing ruthenium salt concentration in the electroplating solution. The XRD pattern of Ru/CP seems difficult to determine, given that the (101) plane of metallic Ru (JCPDS no. 06-0663) overlaps with the peak of CP at around 44°, presumably in the form of amorphous Ru nanoparticles.[30] The Pt/Ru/CP spectrum manifests no significant variation *versus* Pt/CP, confirming no interaction between Pt and Ru by the two-step electrodeposition process, leading to only a slight enhancement in ECH activity. Additionally, the XRD pattern of PtRu/CP-4 after five cycles is almost invariant, proving that the two metals are still present in the form of alloys (Fig. S18†) and the electrode attains high stability.

The X-ray photoelectron spectroscopy (XPS) spectrum explores the surface chemical states of the samples and further confirms the development of the PtRu alloy. The Pt 4f core level in the spectrum of Pt/CP displays the spin–orbit doublet peaks of 4f 7/2 and 4f 5/2 (Fig. 3b), wherein after deconvolution into two pairs of doublets of each peak, the binding energies at around 71.3 eV and 74.7 eV correspond to the metallic state Pt.[8,31] Compared with Pt/CP, the binding energy of Pt^0 is slightly shifted to a higher position in PtRu/CP-4, which is the optimized catalyst with the highest hydrogenation activity. The XPS spectra of the Ru 3p 3/2 region are shown in Fig. 3c with deconvolution into two distinguishable peaks of metallic and oxidized Ru, where the peak of Ru^0 is slightly shifted to the lower-energy orientation in PtRu/CP-4 (Ru $3p_{3/2}$: 462.1 eV) compared with that in Ru/CP (Ru $3p_{3/2}$: 462.3 eV). These shifts are interpreted as the electron transfer from Pt to Ru, suggesting the existence of alloys.[28] The incorporation of Ru possibly exerts bimetallic synergistic effects due to the modification of the electronic structure, thus endowing PtRu/CP-4 with a dramatic leap over Pt/CP for the ECH of benzoic acid. The Pt^0/Pt^{2+} ratio improves from 57/43 to 70/30 after Pt alloying with Ru, and the Ru^0/Ru^{4+} ratio also enhances from 31/69 of Ru/CP to 49/51 of PtRu/CP-4, revealing that the metal on the surface of PtRu/CP-4 exists more in the metallic state, which may also be responsible for the higher activity. XPS analysis shows an atomic Pt : Ru ratio of 5.01 : 1 on the surface of PtRu/CP-4.

The morphologies of Pt/CP and PtRu/CP-*X* are evaluated by scanning electron microscopy (SEM) and applied to explain the correlation between the structure of electrocatalysts and reaction properties. The SEM images of all samples at different magnifications display that the surface fibers of CP are interconnected and catalyst particles are attached on the surface, constituting a hierarchical one-dimensional (1D) structure (Fig. 4a and S19–21†), which attains more intimate contact between the catalyst and electrolyte with open space and provides an adequate amount of accessible active sites at the three-phase interface, developing rapid mass transfer.[32] Efficient electronic transmission is beneficial for improving catalytic ability during the ECH process. The morphology and size of metal nanoparticles for Pt/CP are not uniform through the CV electrodeposition method (Fig. S19†). Interestingly, the catalysts after alloying Pt and Ru are wrapped around the surface of CP and uniformly present as spherical nanoclusters, and with the increase of Ru ion concentration in the electroplating solution, the size of the nanoclusters gradually reduces. The alloy nanoclusters of PtRu/CP-2 exist in the range of 80 and 150 nm (Fig. S20†), and these larger particles may lessen the active sites. Considering the exposure of carbon fibers, the catalyst diameter of PtRu/CP-6 is too small to cover the surface of the support (Fig. S21†), accordingly representing a pronounced decrease in activity. The particle size of PtRu/CP-4 is approximately 20–30 nm (Fig. 4b), namely, PtRu/CP-4 possesses the appropriate diameter nanoclusters and the narrowest particle size distribution to entirely encompass the carbon fiber, endowing the largest ECSA and providing more active sites for the capture of substrate molecules. This uniform structure also ensures high conductivity with the lowest R_{ct} and guarantees the best performance for the ECH of benzoic acid. Elemental mapping by energy-dispersive X-ray spectroscopy (EDX) is performed to analyze the distribution and proportions of elements on the as-obtained samples (Table S2†), demonstrating that the Ru content in the alloy catalyst rises as the concentration of Ru salt in the electroplating solution increases and two metallic elements are homogeneously dispersed on the macro level. The result shows an atomic Pt : Ru ratio of 5.58 : 1 on the surface of the optimized PtRu/CP-4, relatively in line with XPS and inductively coupled plasma atomic emission spectroscopy (ICP-AES) analysis (Table S2†). Moreover, the electrode surface morphology exhibits spherical nanoclusters anchored on carbon fibers without a significant change as shown in SEM images (Fig. S22†), indicating no agglomeration of active ingredients. The composition of surface metal elements (Pt : Ru = 5.26 : 1) is also virtually identical to that of the freshly prepared electrode.

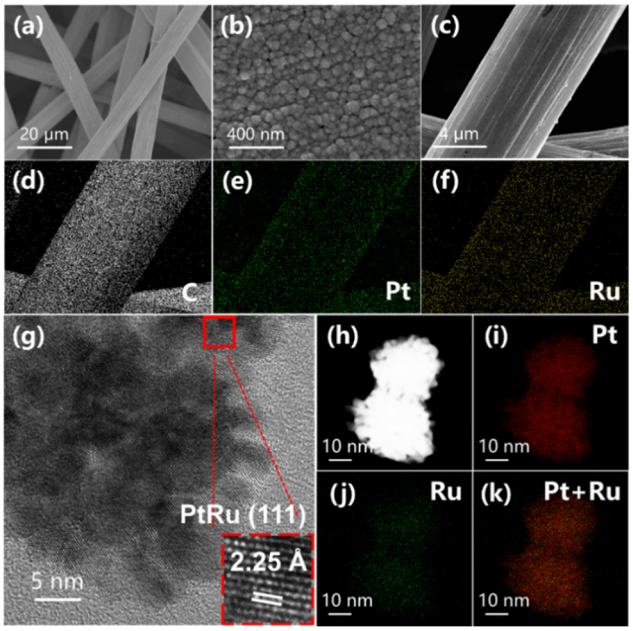

Fig. 4 (a and b) SEM images, (c–f) EDX mapping and (g) TEM image of PtRu/CP-4. (h) STEM and (i–k) EDX mapping of PtRu nanoparticles.

The transmission electron microscopy (TEM) images also unveil the discrimination in the morphology of Pt/CP and PtRu/CP-4. The monometallic Pt nanoclusters are generously sized (>50 nm) and irregularly shaped (Fig. S23†). PtRu/CP-4 is composed of more uniform spherical nanoclusters (20–30 nm) stacked by small nanoparticles (Fig. 4h). The nanoclusters on Pt/CP show a *d*-spacing of 2.27 Å for a crystal lattice, matching the (111) plane of metallic Pt. Whereas there is an explicit lattice contraction for PtRu/CP-4 (interplanar spacing of 2.25 Å), suggesting the formation of an alloy phase between Pt and Ru (Fig. 4g). The elemental distribution of the PtRu alloy is investigated by STEM-EDX analysis (Fig. 4h–k), revealing that Pt and Ru elements are uniformly distributed on CP.

In situ Raman spectroscopy is conducted with current control to uncover the impact of the alloy catalyst and the equipment for measurement is shown in Fig. S24.† Pt/CP, Ru/CP, and PtRu/CP-4 are employed to research the adsorption behavior of benzoic acid. The Raman spectra of benzoic acid are collected on the electrode surface at no current and −3 mA. Benzoic acid displays two characteristic bands at ~1350 cm^{-1} and ~1610 cm^{-1} for three electrocatalysts, representing the carboxyl group and benzene ring, respectively.[23] For Pt/CP, the location of benzene shows a red shift of ~10 cm^{-1} at a current of −3 mA, and the carboxyl group remains unchanged, indicating the strong adsorption of the benzene ring on Pt/CP and the weak adsorption of the carboxyl group (Fig. 5a). This consequence is in accordance with the high selectivity of aromatic hydrogenation products in ECH. The typical bands of two functional groups are barely shifted over Ru/CP (Fig. S25†), explaining the poor reactivity. Interestingly, the peak of the benzene ring exhibits a more tangible red shift of 20 cm^{-1} at −3 mA on PtRu/CP-4 than that on Pt/CP, showing a greater stretching and weakening of the bonds between C atoms in the phenyl ring attributed to the synergistic effect; therefore the conversion of benzoic acid is significantly improved using PtRu/CP-4 (Fig. 5b). The ratio of peak intensities for aromatic and carboxyl groups over PtRu/CP-4 is 2.28, more than twice as high as over Pt/CP (1.10); namely, the alloyed structure assists in the adsorption of the aromatic ring. Fig. 5c visually summarizes the above observation. The Raman spectra of benzoic acid over three electrocatalysts at different potentials are also collected. With the variation of the applied potential from the open circuit potential (OCP) to −0.25 V (*vs.* Ag/AgCl), the intensity of peaks for benzene and carboxyl groups over Pt/CP and PtRu/CP-4 is significantly enhanced, indicating the stronger adsorption of benzoic acid by the electric field (Fig. 5d). For PtRu/CP-4, the peak intensity attributed to the aromatic ring is distinctly greater than that of carboxyl groups with the increase of potential, especially at −0.25 V, which behaves differently from the signal on Pt/CP with no major variation between the benzene and carboxyl groups (Fig. S26a†). These also indicate that more benzoic acid molecules adsorb on the surface of PtRu/CP-4. In comparison, Ru/CP possesses a weak signal overall and the applied potential value has no influence on the peak intensity (Fig. S26b†), indicating the poor adsorption capacity of benzoic acid molecules, which corresponds well to the ECH results.

DFT calculations proceed to deeply identify the reason for the better catalytic performance observed on PtRu/CP-4. The conformation of PtRu/CP-4 is developed based on a Pt–Ru atomic ratio of 5.4 : 1, herein denoted as PtRu (111). The Pt (111) surface is also calculated for comparison. As shown in Fig. S27,† a sequence of alloy models is established to calculate the energy, and the most stable structure is determined as the representative of PtRu (111). Initially, parallel and vertical adsorption structures of benzoic acid on Pt (111) and PtRu (111) are constructed and optimized, respectively. The adsorption energies (E_{ad}) of benzoic acid adsorbed in a parallel manner on Pt (111) and PtRu (111) are calculated to be −2.17 and −2.49 eV, which are much larger than the vertical mode of −0.75 and −0.77 eV (Fig. 6a). This implies that benzoic acid employs aromatic rings forming a mixed σ–π interaction with metal atoms rather than carboxyl groups being adsorbed; consequently, the bonds between the C atoms of the phenyl ring can be selectively activated, which provides a good interpretation for the high selectivity of cyclohexanecarboxylic acid and no carboxyl hydrogenation on both catalysts. It is noteworthy that the aromatic ring of benzoic acid is not arranged exclusively parallel to the surface of the catalyst, but with slanted hydrogen atoms and carboxyl groups.[33] The variation of the bond length presented in Table S3† also clarifies the stretching of the bonds and the adsorption of metal atoms onto benzoic acid molecules. The stronger benzoic acid adsorption in parallel mode on PtRu (111) than that on Pt (111) evidences the existence of a synergistic effect between Pt and Ru atoms promoting the conversion of benzoic acid, which agrees with the

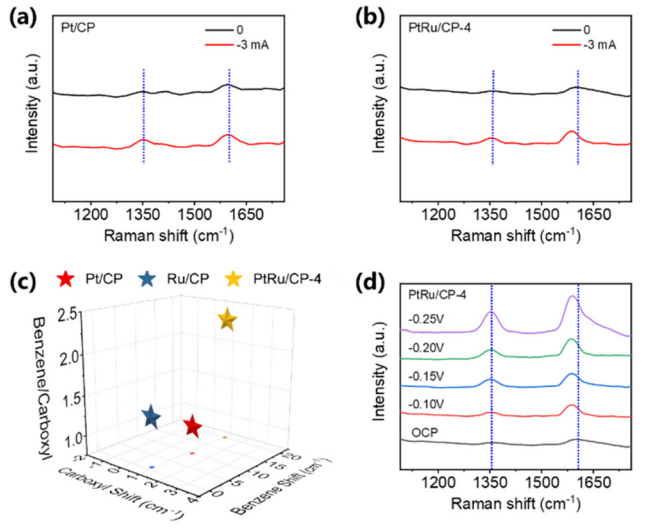

Fig. 5 *In situ* Raman spectra for (a) Pt/CP, and (b) PtRu/CP-4 at no current control and −3 mA. (c) Comparison of Pt/CP, Ru/CP and PtRu/CP-4. The *X*-axis represents the carboxyl shift. The *Y*-axis represents the benzene ring shift. The *Z*-axis represents the ratio of the peak intensity for carboxyl and benzene rings. (d) Potential-dependent Raman spectra for PtRu/CP-4 under open circuit potential (OCP) and different applied potentials (*vs.* Ag/AgCl). Conditions: 0.2 M H_2SO_4, 10 mM benzoic acid.

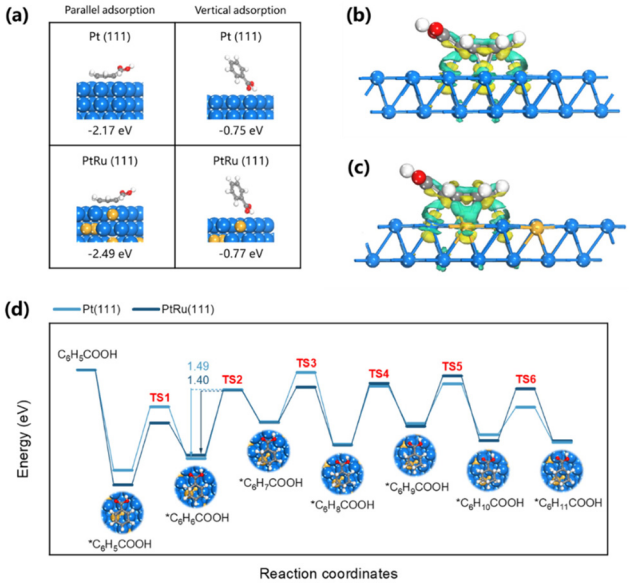

Fig. 6 (a) Different adsorption configurations on Pt(111) and PtRu(111). The charge density difference analysis of benzoic acid on (b) Pt(111) and (c) PtRu(111). The green and yellow colors substitute the charge accumulation and depletion regions, respectively. The isosurface level is all the same, equal to 0.03 e Å^{-3}. (d) The relative energy diagram for the ECH of benzoic acid with the schematic top view of the corresponding reactants on the PtRu(111) surface.

experimental results. The capacity of PtRu (111) and Pt (111) to adsorb protons is further analyzed. It is generally believed that the H atom favors adsorption on the hollow sites of metal surfaces.[34] Therefore, the models are established and optimized to derive stable configurations as shown in Fig. S28.† The E_{ad} of the H atom on Pt (111) (−0.50 eV) is not as strong as that on PtRu (111) (−0.52 eV). Higher H adsorption energy may accelerate the Volmer step to generate H_{ad}, which plays a fundamental role as the source of hydrogen for ECH. Overall, these results explicitly substantiate that the preeminent ECH performance of PtRu/CP-4 can be assigned to the ability of the alloyed structure to simultaneously improve the capture of benzoic acid molecules and interfacial active hydrogen species over the electrocatalysts.

The charge density difference plots featured in Fig. 6b and c indicate distinctive electron transfer initiated by the adsorbed benzoic acid on PtRu (111) and Pt (111). The carboxyl group (electron-accepting group) linked to the aromatic ring (electron-donating group) may degrade the electron density of phenyl, thus strongly adsorbing onto the metal surface. After the adsorption of benzoic acid molecules, more accumulation of electrons around the Ru atom reduces the electron density of the aromatic ring, thereby facilitating the activation of the reaction. From the above, the synergistic interaction between Pt and Ru atoms boosts the conversion of benzoic acid, originating from the fact that Ru is employed to modify the electronic structure of Pt. The first hydrogenation started with transferring a surface-adsorbed H atom to benzoic acid, and six different attachments including the *ortho*-, *meta*-, and *para*-sites of the carboxyl group according to the continuous hydrogenation process[33,34] are calculated and compared in Fig. S29.† The *ortho*-$C_6H_6COOH(C_6)$ is the most stabilized structure and the subsequent hydrogenation adheres to the sequence of C_5–C_4–C_3–C_2–C_1 (Fig. S29†). Upon calculation (Fig. 6d), the second step of hydrogenation (C_6H_6COOH to C_6H_7COOH) possesses the highest energy barriers throughout the whole process, in line with the conclusion by Peng[11] that the rate-determining step of aromatic ring hydrogenation is the addition of the first pair of hydrogen atoms. The activation barriers on Pt (111) and PtRu (111) are 1.40 and 1.49 eV, respectively. Consequently, it is emphasized that the high activity of PtRu (111) is due to the reduced activation barrier of the most energy-consuming step. Apart from verifying the experimental results, the theoretical calculations define the beneficial role of Ru and explain the reason for the high efficiency of the PtRu alloy in the ECH of benzoic acid.

As shown in Fig. 7, the reaction mechanism over PtRu/CP-4 is summarized based on the above results and the previous report.[27] It should be noted that the L–H mechanism is generally believed to be the ECH pathway of organics with benzene rings, *e.g.*, the hydrogenation of phenol[27] and benzaldehyde[34] on the platinum-group catalysts, where adsorbed H atoms generated by the electrolysis of water react with the adsorbed organics on the catalyst surface, with subsequent desorption of the products from the cathode to the electrolyte. During the ECH process of benzoic acid, H^+ is readily captured to produce H_{ad} due to the highly efficient electronic transmission arising from the uniform electrodeposition of alloy nanoclusters and the synergistic interactions between Pt and Ru atoms. As Ru modifies the electronic structure of Pt, the adsorption capacity of the catalyst onto benzoic acid is dramatically elevated. Afterward, H_{ad} is rapidly transferred to benzoic acid molecules on the surface of the catalyst and the ECH reaction occurs. The synergistic effect is likewise preferential in that it lowers the energy barrier of benzoic acid hydrogenation and accelerates the reaction rate. It is worth noting that the aromatic ring of benzoic acid is deemed as the capture pattern rather than the carboxyl group, thus favoring the high selectivity of cyclohexanecarboxylic acid with no by-product.

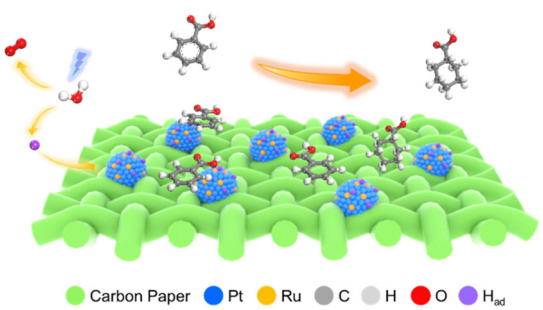

Fig. 7 The possible mechanism for the ECH of benzoic acid over PtRu/CP-4.

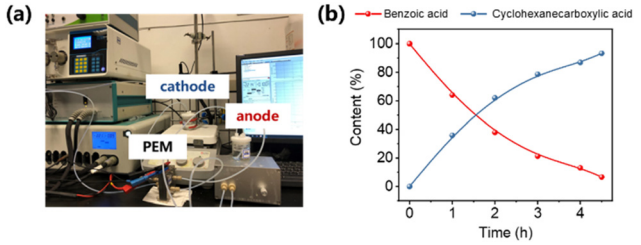

Fig. 8 (a) The photograph of the ECH electrolyzer cell and reaction system. (b) Relative content of benzoic acid and cyclohexanecarboxylic acid. Conditions: 0.2 M H_2SO_4, 10 mM benzoic acid, −100 mA, room temperature.

To determine the practical application of PtRu/CP-4, a proton-exchange membrane reactor is adopted for the ECH of benzoic acid and the OER, thereby achieving the purpose of flow feeding. PtRu/CP-4 (2.0 cm × 2.0 cm) and Pt foil located on each side of the Nafion 117 membrane are cathode and anode, respectively, and the physical image of the reaction system is shown in Fig. 8a and S30.† Both chambers of the electrolyzer are combined with peristaltic pumps and the electrolyte tank. The electrolytes (100 mL anolyte and catholyte containing 0.2 M H_2SO_4 and 0.2 M H_2SO_4 with 10 mM benzoic acid, respectively) are circulated by the pump with an optimized flow rate of 100 mL min^{-1}. Constant current electrolysis is performed in a two-electrode system at −100 mA. Over 90% of benzoic acid generates cyclohexanecarboxylic acid within 4.5 h in a nearly invariant voltage range of −2.2 to −2.3 V, implying the high stability of this reaction system (Fig. 8b). Such inspiring results emphasize the potential of PtRu/CP-4 for large-scale production of fine chemicals *via* electrosynthesis.

Conclusions

In summary, uniform PtRu bimetallic nanoclusters electrodeposited on carbon paper (CP) catalysts are prepared for the electrochemical hydrogenation of aromatic rings in benzoic acid derivatives, wherein optimized PtRu/CP-4 maintains an inspiring high conversion of 92.9%, high selectivity of 100%, and a high FE of 62.2% in an acidic aqueous electrolyte without using external H_2. The outstanding stability and wide substrate scope also indicate the superiority of the PtRu bimetallic catalyst. Electrodeposition effectively strengthens the combination of PtRu bimetallic active sites and carbon fibers to promote electron transmission, while avoiding the aggregation of bimetallic nanoclusters to enhance their stability in acidic environments. Given that Ru modifies the electronic structure of Pt, the synergistic effect is capable of simultaneously improving the capture of benzoic acid molecules and interfacial active hydrogen species. After adsorbing benzoic acid, more accumulation of electrons around the Ru atom reduces the electron density of the aromatic ring, thereby facilitating the activation of the reaction. Moreover, the PtRu bimetallic catalyst is preferentially used to reduce the energy barrier of benzoic acid hydrogenation and accelerate the reaction rate. The large-scale ECH of benzoic acid to cyclohexanecarboxylic acid is also tested using a continuous proton-exchange membrane reactor, emphasizing its potential for producing value-added chemicals *via* electrosynthesis. This work provides a highly efficient strategy for the hydrogenation of aromatic rings in benzoic acid derivatives under mild and environmentally-friendly conditions.

Experimental

Materials

CP (TGPH-060) was produced by Toray. $H_2PtCl_6{\cdot}6H_2O$ and Ru $(NO)(NO_3)_x(OH)_y$, $x + y = 3$, (Ru 1.5% w/v) were obtained from Aladdin and Macklin, respectively. Nafion-117 (DuPont, America) was used to separate the cathode and anode compartments. Benzoic acid (99.5%), cyclohexanecarboxylic acid (99%), *o*-methyl benzoic acid (98%), *m*-methyl benzoic acid (>99.0%), *p*-methyl benzoic acid (98%), *o*-ethyl benzoic acid (97%), *o*-trifluoromethylbenzoic acid (98%), phthalic acid (99%), phthalide (99%), 1-naphthoic acid (98%), methyl benzoate (99%), anisole (98%), and *n*-dodecane (>99.0%) were purchased from Aladdin. Sulfuric acid (95–98%) and ethyl acetate (≥99%) were produced by Tianjin Kemiou Chemical Reagent Co., Ltd.

Synthesis of PtRu/CP electrocatalysts

CP was cut into 1.5 cm × 2 cm pieces, and then washed with acetone, ethanol, and DI water under ultrasonic treatment. First, CP was subjected to hydrophilic treatment *via* an electrical activation method using an Autolab PGSTAT302N/FRA electrochemical workstation. The treatment was conducted in a three-electrode system equipped with a clean CP as the working electrode, a saturated calomel electrode (SCE) as the reference electrode, and a carbon rod as the counter electrode at −2.0 V for 60 s for each side of CP in 0.2 M K_2SO_4, and finally washed with DI water. Typically, bimetallic PtRu catalysts were synthesized by co-electrodeposition onto CP in a three-electrode system (Scheme 1).[11,16,18] The setup of electrodes was the same as above. Electrodeposition was performed by CV, which was subjected to a range of potentials between −0.5 and 1.7 V at a scan rate of 0.1 V s^{-1} for 20 cycles. The surface area of all prepared electrodes immersed in the electrolyte was controlled to 1.5 cm × 1.5 cm (*ca.* 0.0210 g). All electrolytes consisted of an aqueous 0.5 M Na_2SO_4 solution as the supporting electrolyte. 2 mM, 4 mM, and 6 mM Ru salt solutions were added to 10 mM of H_2PtCl_6 as the electroplating solution, respectively, and recorded as PtRu/CP-2, PtRu/CP-4, and PtRu/CP-6. The mass difference was ~1.2 mg before and after electrodeposition. As a control, a Pt/Ru/CP electrode was prepared by a step-by-step electrodeposition method. Primarily, the Ru atoms were electrochemically fabricated on the CP surface in 4 mM Ru salt solution. Subsequently, the Pt atoms were deposited on the Ru/CP electrodes in a solution of

10 mM H_2PtCl_6. The monometallic catalysts (Pt/CP, Ru/CP) were prepared using a 10 mM corresponding metal solution. After these processes, the obtained working electrodes were washed with DI water and dried in the air. In addition, PtRu/CP-4 (2.0 cm × 2.0 cm) used in the PEM reactor for large-scale application was prepared by CV co-electrodeposition for 50 cycles.

Catalyst characterization

The XRD of the prepared electrodes was investigated using a Rigaku SmartLab 9 kW diffractometer with Cu Kα_1 radiation at a voltage of 240 kV and a current of 50 mA. The 2θ angular regions were determined between 30° and 90° at a scan rate of 20° min^{-1}. XPS (ESCALAB250 Surface Science) was used to characterize the electronic states of catalysts with an exciting source of Al Kα = 1486.6 eV. The binding energies were corrected for specimen charging by referencing C 1s to 284.6 eV. The morphology of the electrodes and EDX were acquired by SEM using a Hitachi UHR FE-SEM SU8220. TEM patterns were obtained over a JEOL JEM-F200. The loading amount of Pt and Ru on the electrodes was measured by ICP-AES on a PerkinElmer AVIO 500 device. *In situ* Raman spectra were recorded on a Thermo Fisher DXR Raman spectrometer. A simple flow cell reactor as the reaction equipment for measurement is shown in Fig. S30,† where the as-obtained electrocatalysts served as the cathode, a Pt wire was applied as the anode, and the reference electrode was Ag/AgCl. The Raman spectra of benzoic acid were collected on the different electrode surfaces at no current, −3 mA, and applied potential from OCP to −0.25 V (*vs.* Ag/AgCl).

Electrochemical measurements

Electrochemical measurements were performed using an Autolab PGSTAT302N/FRA at room temperature, which consisted of a three-electrode system with the prepared electrodes, a platinum sheet, and an Ag/AgCl (in saturated KCl solution) as the working, counter, and reference electrodes, respectively. The potential *vs.* Ag/AgCl was converted to the potential *vs.* RHE based on the Nernst equation:

$$E_{RHE} = E_{Ag/AgCl} + 0.059 \times pH + 0.198\ V. \quad (1)$$

All solutions were purged with N_2 to remove dissolved O_2 before the experiments. LSV tests were recorded with 70% *iR* compensation at a scan rate of 5 mV^{-1} in 0.2 M H_2SO_4 with and without benzoic acid. CV proceeded in 0.2 M H_2SO_4 within a non-faradaic region for calculating C_{dl}, which determined the ECSA of the prepared electrodes. EIS tests were conducted in the presence of benzoic acid at a frequency of 10^5–10^{-1} Hz with an AC voltage of 10 mV.

Electrocatalytic hydrogenation of benzoic acid derivatives

Electrocatalytic activity tests were performed with the same three-electrode system in a 25 mL H-type cell separated by Nafion 117. The prepared electrodes (1.5 cm × 1.5 cm), a platinum foil electrode (2.5 cm × 2.5 cm), and an Ag/AgCl (in saturated KCl solution) electrode with a salt bridge served as the working, counter, and reference electrodes respectively. The prepared electrodes were polarized for 10 min at a constant current of −50 mA before electrocatalytic reaction tests, where both the anode and cathode chambers contained 0.2 M H_2SO_4. Subsequently, benzoic acid was added into the cathode compartment until it was wholly dissolved for a final concentration of 10 mM, followed by galvanostatic electrolysis with a specified current at room temperature (certain benzoic acid derivatives were electrolyzed at 50 °C, and the specific reaction conditions for substrate scopes are shown in Table 2). During the stability experiment, PtRu/CP-4 was washed with DI water and ethanol after each cycle, and the electrolyte was substituted with a fresh one. After the reaction, 1 mL of the cathodic solution was collected and extracted with 2 mL of ethyl acetate, which contained *n*-dodecane as the internal standard. The liquid samples were analyzed using an Agilent GC 8890A with a FID (HP-5 capillary column, 0.25 μm × 0.32 mm × 30 m), and the correction factor by standard materials was calculated. The carbon balance of all reaction results was above 95%. The products for the hydrogenation of benzoic acid derivatives were detected by GC-MS on an Agilent 7890/5973 equipped with MSD ChemStation software. The evaluation indicators were calculated based on the following equations:

$$\text{Conversion of benzoic acid}(\%) = \frac{\text{mol of benzoic acid consumed}}{\text{mol of initial benzoic acid}} \times 100\% \quad (2)$$

$$\text{Selectivity to } X(\%) = \frac{\text{mol of } X \text{ formed}}{\text{mol of all identified products}} \times 100\% \quad (3)$$

$$\text{FE}(\%) = \frac{\text{mol of formed}}{\text{total charge passed}(C)/(F \times n)} \times 100\% \quad (4)$$

$$\text{Space} - \text{time yield}\left(\text{g m}^{-3}\ \text{h}^{-1}\right) = \frac{\text{quantity of cyclohexanecarboxylic acid}(g)}{\text{reactor volume}(\text{m}^3) \times \text{reaction time}(\text{h})} \quad (5)$$

$$\text{Carbon balance}(\%) = \frac{\text{mol of all products} + \text{mol of remaining benzoic acid}}{\text{mol of initial benzoic acid}} \quad (6)$$

where X is the reaction product, F is the faradaic constant (96 485 C mol^{-1}), and n is the number of electrons required for product formation (n = 6 for benzoic acid to cyclohexanecarboxylic acid and other benzoic acid derivatives to its benzene ring hydrogenation products).

DFT calculations

All calculations were carried out using Materials Studio software 19.1 with the program package DMol^3. The generalized-gradient approximation (GGA) with the Perdew–Burke–Ernzerhof (PBE) functional described the exchange–correlation energy. In configuration optimization, the parameters of the tolerance for the self-consistent field (SCF), energy, maximum force, and maximum displacement were set to 1.0 × 10^{-5}

Hartree, 1.0×10^{-5} Hartree, 0.002 Hartree per Å and 0.005 Hartree per Å, respectively. To enhance computational performance, all calculations were performed with a thermal smearing of 0.005 Ha and spin polarization. 4-Layer 4 × 4 Pt (111) and PtRu (111) slabs were built with a 20 Å vacuum gap and fixed bottom two layers. A (2 × 2 × 1) *k*-point grid was set, and the TS method was used for DFT-D correction. The E_{ad} of the different adsorbates is defined as:

$$E_{ad} = E_{total} - (E_{adsorbate} + E_{baresurface}) \quad (7)$$

where E_{total} shows the total energy of the slab after adsorption, $E_{adsorbate}$ is the energy of an adsorbate molecule, and $E_{bare\ surface}$ is the energy of the bare metal surface.

Conflicts of interest

There are no conflicts to declare.

Acknowledgements

This research is supported by the National Natural Science Foundation of China (22172016, 22272014, and 22161132005), the Science and Technology Innovation Fund in Dalian City (2021J12GX025), and the Fundamental Research Funds for the Central Universities (DUT2021TD03 and DUT21LK02). We are grateful for the guidance of DFT calculations by Dr Shengnan Bi.

References

1 B. S. Moore, H. Cho, R. Casati, E. Kennedy, K. A. Reynolds, U. Mocek, J. M. Beale and H. G. Floss, *J. Am. Chem. Soc.*, 1993, **115**, 5254–5266.
2 X. Xu, M. Tang, M. Li, H. Li and Y. Wang, *ACS Catal.*, 2014, **4**, 3132–3135.
3 M. Guo, X. Kong, C. Li and Q. Yang, *Commun. Chem.*, 2021, **4**, 54.
4 M. Tang, S. Mao, M. Li, Z. Wei, F. Xu, H. Li and Y. Wang, *ACS Catal.*, 2015, **5**, 3100–3107.
5 H. Miyamura, A. Suzuki, T. Yasukawa and S. Kobayashi, *J. Am. Chem. Soc.*, 2018, **140**, 11325–11334.
6 Y. Hu, W. Chen, Y. Chen, F. Zhang, W. Song, L. Wang, J. Fu, X. Ren, S. You, C. Cao, Z. Yu and X. Dong, *Catal. Lett.*, 2022, **152**, 2164–2177.
7 X. Chen, Z. Wang, H. Daly, R. Morgan, H. Manyar, C. Byrne, A. S. Walton, S. F. R. Taylor, M. Smith, R. Burch, P. Hu and C. Hardacre, *Appl. Catal., A*, 2020, **593**, 117420.
8 H. Zhang, J. Dong, X. Qiao, J. Qin, H. Sun, A. Wang, L. Niu and G. Bai, *J. Catal.*, 2019, **372**, 258–265.
9 X. H. Lu, Y. Shen, J. He, R. Jing, P. P. Tao, A. Hu, R. F. Nie, D. Zhou and Q. H. Xia, *Mol. Catal.*, 2018, **444**, 53–61.
10 R. Wu, Q. Meng, J. Yan, H. Liu, Q. Zhu, L. Zheng, J. Zhang and B. Han, *J. Am. Chem. Soc.*, 2022, **144**, 1556–1571.
11 T. Peng, T. Zhuang, Y. Yan, J. Qian, G. R. Dick, J. Behaghel de Bueren, S.-F. Hung, Y. Zhang, Z. Wang, J. Wicks, F. P. Garcia de Arquer, J. Abed, N. Wang, A. Sedighian Rasouli, G. Lee, M. Wang, D. He, Z. Wang, Z. Liang, L. Song, X. Wang, B. Chen, A. Ozden, Y. Lum, W. R. Leow, M. Luo, D. M. Meira, A. H. Ip, J. S. Luterbacher, W. Zhao and E. H. Sargent, *J. Am. Chem. Soc.*, 2021, **143**, 17226–17235.
12 M. Garedew, D. Young-Farhat, J. E. Jackson and C. M. Saffron, *ACS Sustainable Chem. Eng.*, 2019, **7**, 8375–8386.
13 C. Tang, Y. Zheng, M. Jaroniec and S.-Z. Qiao, *Angew. Chem., Int. Ed.*, 2021, **60**, 19572–19590.
14 H. Liu, D. M. Patel, Y. Chen, J. Lee, T.-H. Lee, S. D. Cady, E. W. Cochran, L. T. Roling and W. Li, *ACS Catal.*, 2022, **12**, 14072–14085.
15 G. Chen, L. Liang, N. Li, X. Lu, B. Yan and Z. Cheng, *ChemSusChem*, 2021, **14**, 1037–1052.
16 M. Wang, T. Peng, C. Yang, B. Liang, H. Chen, M. Kumar, Y. Zhang and W. Zhao, *Green Chem.*, 2022, **24**, 142–146.
17 S. Wang, K. Uwakwe, L. Yu, J. Ye, Y. Zhu, J. Hu, R. Chen, Z. Zhang, Z. Zhou, J. Li, Z. Xie and D. Deng, *Nat. Commun.*, 2021, **12**, 7072.
18 H. Chen, T. Peng, B. Liang, D. Zhang, G. Lian, C. Yang, Y. Zhang and W. Zhao, *Green Chem.*, 2022, **24**, 3655–3661.
19 P. Zhang, X. Sheng, X. Chen, Z. Fang, J. Jiang, M. Wang, F. Li, L. Fan, Y. Ren, B. Zhang, B. J. J. Timmer, M. S. G. Ahlquist and L. Sun, *Angew. Chem., Int. Ed.*, 2019, **58**, 9155–9159.
20 W. Liu, W. You, Y. Gong and Y. Deng, *Energy Environ. Sci.*, 2020, **13**, 917–927.
21 Y. Zhou, Y. Gao, X. Zhong, W. Jiang, Y. Liang, P. Niu, M. Li, G. Zhuang, X. Li and J. Wang, *Adv. Funct. Mater.*, 2019, **29**, 1807651.
22 A. Fukazawa, Y. Shimizu, N. Shida and M. Atobe, *Org. Biomol. Chem.*, 2021, **19**, 7363–7368.
23 A. Kong, M. Liu, H. Zhang, Z. Cao, J. Zhang, W. Li, Y. Han and Y. Fu, *Chem. Eng. J.*, 2022, **445**, 136719.
24 Y. Du, X. Chen and C. Liang, *Mol. Catal.*, 2023, **535**, 112831.
25 Y. Hu, W. Chen, Y. Chen, F. Zhang, W. Song, L. Wang, J. Fu, X. Ren, S. You, C. Cao, Z. Yu and X. Dong, *Catal. Lett.*, 2022, **152**, 2164–2177.
26 M. Tang, S. Mao, M. Li, Z. Wei, F. Xu, H. Li and Y. Wang, *ACS Catal.*, 2015, **5**, 3100–3107.
27 N. Singh, U. Sanyal, G. Ruehl, K. A. Stoerzinger, O. Y. Gutiérrez, D. M. Camaioni, J. L. Fulton, J. A. Lercher and C. T. Campbell, *J. Catal.*, 2020, **382**, 372–384.
28 J. Zhu, F. Cheng, Z. Tao and J. Chen, *J. Phys. Chem. C*, 2008, **112**, 6337–6345.
29 H. J. Kim, S. M. Choi, S. Green, G. A. Tompsett, S. H. Lee, G. W. Huber and W. B. Kim, *Appl. Catal., B*, 2011, **101**, 366–375.
30 X. Hu, J. Zou, H. Gao and X. Kang, *J. Colloid Interface Sci.*, 2020, **570**, 72–79.
31 M. Zhu, B. Huang, Q. Shao, Y. Pi, Y. Qian and X. Huang, *ChemCatChem*, 2018, **10**, 3214–3218.

32 Y. Zhong, R. Ren, Y. Peng, J. Wang, X. Ren, Q. Li and Y. Fan, *Mol. Catal.*, 2022, **528**, 112487.
33 G. Li, J. Han, H. Wang, X. Zhu and Q. Ge, *ACS Catal.*, 2015, **5**, 2009–2016.
34 L. Zhou, X. Zhu, H. Su, H. Lin, Y. Lyu, X. Zhao, C. Chen, N. Zhang, C. Xie, Y. Li, Y. Lu, J. Zheng, B. Johannessen, S. P. Jiang, Q. Liu, Y. Li, Y. Zou and S. Wang, *Sci. China: Chem.*, 2021, **64**, 1586–1595.